Computers in Biology and Medicine 194 (2025) 110427

Contents lists available at ScienceDirect

Computers in Biology and Medicine

journal homepage: www.elsevier.com/locate/compbiomed

Geometric immunosuppression in CAR T-cell treatment: Insights from mathematical modeling

Silvia Bordel-Vozmediano [a,b,*], Soukaina Sabir [a,b], Lucía Benito-Barca [c], Bettina Weigelin [d,e], Víctor M. Pérez-García [a,b]

[a] Mathematical Oncology Laboratory (MOLAB), Instituto de Matemática Aplicada a la Ciencia y la Ingeniería, Universidad de Castilla-La Mancha, Ciudad Real, 13005, Spain
[b] Departamento de Matemáticas, Escuela Técnica Superior de Ingenieros Industriales, Universidad de Castilla-La Mancha, 13005, Ciudad Real, Spain
[c] Facultad de Ciencias Experimentales, Universidad Francisco de Vitoria, Pozuelo de Alarcón, 28223, Spain
[d] Department of Preclinical Imaging and Radiopharmacy, Multiscale Immunoimaging, Eberhard Karls University, Tübingen, Germany
[e] Cluster of Excellence iFIT (EXC 2180) "Image-Guided and Functionally Instructed Tumor Therapies", Eberhard Karls University, Tübingen, Germany

ARTICLE INFO

Dataset link: https://github.com/sibordel/CellularAutomataCAR-T.git

Keywords:
CAR T-cell
Cellular automata
Immunotherapy
Tumor geometry
Spatial dynamics

ABSTRACT

Chimeric antigen receptor T (CAR T) cell therapy has emerged as a promising treatment for hematological malignancies, offering a targeted approach to cancer treatment. Understanding the complexities of CAR T-cell therapy within solid tumors poses challenges due to the intricate interactions within the tumor microenvironment. Mathematical modeling may serve as a valuable tool to unravel the dynamics of CAR T-cell therapy and improve its effectiveness in solid tumors. This study aimed to investigate the impact of spatial aspects in CAR T therapy of solid tumors, utilizing cellular automata for modeling purposes. Our main objective was to deepen our understanding of treatment effects by analyzing scenarios with different spatial distributions and varying the initial quantities of tumor and CAR T-cells. Tumor geometry significantly influenced treatment efficacy in-silico, with notable differences observed between tumors with block-like arrangements and those with sparse cell distributions, leading to the concept of immune suppression due to geometrical effects. This research delves into the intricate relationship between spatial dynamics and the effectiveness of CAR T therapy in solid tumors, highlighting the relevance of tumor geometry in the outcome of cellular immunotherapy treatments. Our results provide a basis for improving the efficacy of CAR T-cell treatments by combining them with other ones reducing the density of compact tumor areas and thus opening access ways for tumor killing T-cells.

1. Introduction

The advent of immunotherapy is revolutionizing cancer treatment. Among the many different immunotherapies available today, cellular immunotherapies based on modified patient-derived immune cells have emerged as promising concept [1]. Chimeric antigen receptor (CAR) T-cell therapy, one example of cell-based immunotherapies, relies on genetically engineering immune cells to express a synthetic receptor that targets surface antigens on tumor cells. CARs are composed of an antibody-derived extracellular domain that confers high specificity for tumor antigens, linked to intracellular signaling domains that drive *T* cell activation and effector function upon antigen binding. The generation of CAR T-cells begins by isolating *T* cells from the patient's blood, followed by ex vivo activation, expansion and genetic modification to express the CAR receptor. Once reinfused into the patient's bloodstream, CAR T-cells home to lymphatic organs and tumor tissue where they selectively bind to cancer cells expressing the targeted antigen. Upon binding, the CAR receptor triggers the release of cytotoxic vesicles, leading to the destruction of the malignant cells [2,3].

Initially celebrated for its remarkable success in treating hematological malignancies [4,5], CAR T-cell therapy has faced challenges in addressing solid tumors. They are highly heterogeneous, including diverse antigen expression that limits tumor recognition and highly variable tumor microenvironments (TMEs) that inhibit CAR T-cell effector functions [6]. Despite these challenges, recent advancements in CAR T-cell engineering combined with a deeper understanding of tumor biology and immunology have renewed optimism for CAR T-cell success in solid tumors [7,8]. CAR T-cells have e.g., been genetically modified to enhance their effector functions, prolong their survival and

* Corresponding author at: Mathematical Oncology Laboratory (MOLAB), Instituto de Matemática Aplicada a la Ciencia y la Ingeniería, Universidad de Castilla-La Mancha, Ciudad Real, 13005, Spain.
E-mail address: silvia.bordel@uclm.es (S. Bordel-Vozmediano).

https://doi.org/10.1016/j.compbiomed.2025.110427
Received 10 February 2025; Received in revised form 14 May 2025; Accepted 19 May 2025
Available online 11 June 2025

improve their migratory capacity within the TME [9]. However, the complexity and redundancy of immunosuppressive mechanisms still make it challenging to identify which modifications are critical for optimizing CAR T-cell performance in the TME.

Mathematical models, designed to describe, quantify, and predict multifaceted cell behavior, offer great potential for enhancing our understanding of CAR T-cell dynamics in solid tumors. By integrating experimental data and computational simulations, mathematical models may provide insights into the mechanisms underlying CAR T-cell efficacy or failure in the solid tumor microenvironment. Modeling can thus help unravel the interactions between tumor and immune cells in relation to microenvironmental parameters. Consequently, we have witnessed an extensive utilization of mathematical approaches in this domain in recent years. In hematological cancers, such as leukemia and lymphoma, mathematical models have focused on describing the kinetics of CAR T-cell expansion, interaction with tumor cells and the immune microenvironment within the bloodstream and lymphatic system and treatment associated toxicity [10–18]. Models used incorporated parameters such as CAR T-cell proliferation rates, tumor burden, cytokine levels, and immune cell interactions to predict treatment efficacy and potential adverse effects. However, most of those works have developed models of compartmental type and thus assumed implicitly a well mixed population of CAR T and tumor cells which does not reflect the biology of solid tumors. Mathematical modeling of CAR T-cell function in solid tumors presents distinct challenges and models must encompass the varying spatial distribution of tumor cells and CAR T-cells within the tumor, distinct antigen expression levels, and diverse immunosuppressive TME niches. As models available to date have relied on assuming homogeneously mixed cancer and effector cell populations (see e.g. [19–23]), there remains a notable gap in the literature concerning the spatial dynamics of treatment response.

Our study aims to fill this gap by investigating the spatial dynamics of CAR T-cell therapy using cellular automata [24,25]. In recent years, the number of papers using CAs and agent-based models to study tumor growth accounting for immune interactions has been increasing [26–33]. As example, Mallet et al. [29] developed a moderately complex, hybrid cellular automata model combined with a deterministic partial differential equation (PDE). In this model, they investigated the dynamics of tumor–immune system interactions by incorporating natural killer cells and cytotoxic T lymphocytes. They considered immune cell migration, death, and tumor lysis mediated by immune cells. Their findings revealed that depending on the strength of T cell recruitment and T cell killing kinetics, tumors exhibited stable or unstable oscillations, and in some cases, were completely eradicated. Zouhri et al. [34] improved this model by incorporating additional biological aspects such as the effects of interleukin-2 on the immune response.

In our study, we used a cellular automaton (CA) to investigate how the spatial distribution of tumor cells in the TME modulates tumor cell accessibility and consequently impacts CAR T-cell efficacy. We find that the spatial arrangement of tumor cells significantly influences T cell expansion and T cell-mediated tumor elimination. Our study serves as a proof of concept, aiming not to analyze a specific tumor type or CAR T-cell construct but rather to explore the general influence of tumor geometry on CAR T-cell therapy efficacy. While we acknowledge that different tumors express distinct target antigens and that CAR T-cell specificity depends on these markers, our approach was intentionally designed to be broadly applicable across various tumor contexts. By abstracting molecular and antigenic heterogeneity, our model highlights the fundamental role of spatial constraints and tumor architecture in shaping treatment outcomes, irrespective of tumor type or CAR T-cell design.

Although our model retains certain similarities between CAR T-cells and conventional cytotoxic T lymphocytes, particularly in the general concept of serial cytotoxic interactions, we have adapted these features to more accurately reflect the distinct behaviors of CAR T-cells. As described by Weigelin et al. [35,36], both CAR T-cells and T lymphocytes require multiple contacts, or "hits", with tumor cells to induce effective killing—a process known as serial killing. To represent this behavior, we implemented a probabilistic killing mechanism in which each interaction between a CAR T-cell and a tumor cell gradually increases the probability of tumor cell death, in line with the cumulative cytotoxic effects observed in experimental studies [35,36].

In addition, our model incorporates CAR T specific dynamics to account for their distinct biological properties. In particular, CAR T-cell expansion is modeled as being stimulated directly by contact with tumor cells, replicating the antigen-driven proliferation characteristic of CAR T therapy [2,37]. Moreover, we assign higher probabilities of tumor cell killing per interaction to CAR T-cells compared to conventional T cells, capturing their enhanced cytotoxic potency and rapid activation upon antigen engagement.

2. Materials and methods

The primary aim of this study was to explore how different tumor geometries influence the response to CAR T-cell treatment by simulating the interaction between tumor cells and tumor-specific CAR T-cells using cellular automata. We aimed to determine whether tumor cells are equally accessible to CAR T-cells across various geometries and to identify differences in treatment response caused by tumor cell distribution. Achieving this implementation requires careful consideration of the biological rules governing each cell type under investigation (see Fig. 1). Key processes to be incorporated include tumor cell proliferation and apoptosis thresholds as well as the viability and proliferative activity of CAR T-cells and the sustainability of their effector function. The details of all biological rules included in our CA are provided in this section.

2.1. Physical structure

The model consisted of a two-dimensional cellular automata operating on a $m \times m$ square lattice. Most of the simulations were run with $m = 200$, thus a 4×10^4 cell-lattice. Some studies were repeated with $m = 400$ (1.6×10^5 cells) to test the robustness of the results for larger lattice sizes, although always with similar results. Each site, can adopt one of three distinct states: 0 indicates an empty cell, 1 signifies a cell containing a CAR T-cell, and 2 denotes a cell occupied by a tumor cell. CAR T-cells are significantly smaller than typical tumor cells, a well-documented biological characteristic. Studies indicate that T cells generally range between 5 and 10 μm in diameter, whereas tumor cells in solid tumors are considerably larger, with diameters spanning 10 to 20 μm [38–40]. This size disparity serves as the foundation for our modeling approach. Given that the average tumor cell diameter is approximately twice that of a CAR T-cell, we integrated this difference into our cellular automata framework by assigning one grid site to each CAR T-cell, while each tumor cell occupies four adjacent grid sites arranged in a square. This spatial representation ensures consistency with biological measurements: if the width of a single grid cell corresponds to the diameter of a CAR T-cell, then a tumor cell — being twice as large — must extend across two grid cells in each direction, thus covering a total of four adjacent grid sites. Given an average CAR T-cell diameter of approximately 10 μm [38], our spatial domain represents a 4 mm^2 tissue area.

In the model, we used a Moore neighborhood with a radius of 1. It is important to note that tumor cells exhibit a higher degree of neighboring connections compared to CAR T-cells. Each CAR T-cell is surrounded by 8 neighboring cells, while each tumor cell is adjacent to 12 neighboring cells.

Our study considered two distinct geometries for the distribution of tumor cells within the lattice: dense and sparse. In the sparse geometry, tumor cells were randomly distributed throughout the lattice, avoiding physical overlap and scattered uniformly without following a specific clustering pattern. In contrast, the dense tumor geometry involved

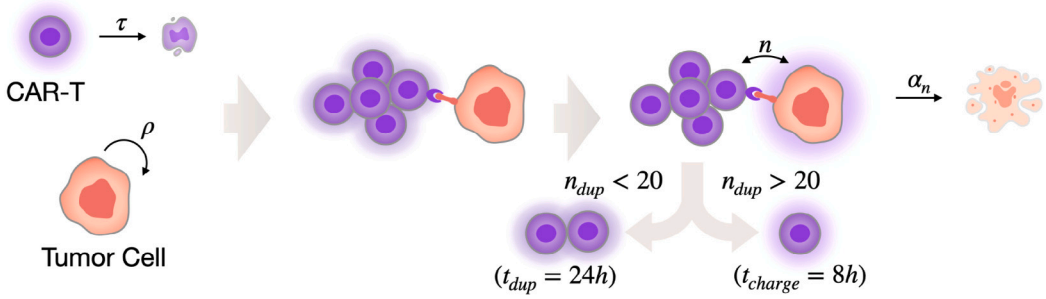

Fig. 1. Biological processes incorporated to the mathematical model. Isolated CAR T-cells have a fixed lifespan, τ, while tumor cells proliferate at a fixed rate ρ. CAR T-cells are allowed to move through the lattice (but not tumor cells). When a CAR T-cell encounters a tumor cell, attaches to it and delivers its cytotoxic load. Tumor cells are capable of accumulating the cytotoxic load from multiple CAR T-cells. The probability of tumor cell death, denoted as α_n, depends on n, which represents the number of CAR T-cells it has interacted with. After interactions between a tumor cell and CAR T-cells, two options arise depending on the value of the duplication counter, n_{dup}. If $n_{dup} < 20$, CAR T-cells that have released their cytotoxic load enter a duplication phase lasting 24 h ($t_{dup} = 24$ h). Upon exiting this phase, CAR T-cells duplicate, with both the mother and daughter cells increasing n_{dup} by 1. If $n_{dup} > 20$, it means that CAR T-cells that have released their cytotoxic load can no longer duplicate because they have reached their maximum capacity. In this case, the CAR T-cell remains stationary, awaiting a recharge of its cytotoxic load, which takes $t_{charge} = 8$ h.

tumor cells clustered in a compact mass located at the center of the lattice, forming a dense and cohesive structure. In both scenarios, CAR T-cells were randomly positioned on the empty lattice sites.

The selection of initial CAR T-cell concentrations in our model was guided by the work of Cooper et al. [41], who developed a hybrid model of the anti-tumor immune response, integrating a cellular automaton and a system of partial differential equations. In their model, they assumed an initial effector T cell concentration of approximately 10^{-6} cells/μm^2. Given the distinct functional advantages of CAR T-cells over conventional effector T cells, such as enhanced antigen specificity, increased cytotoxicity, robust proliferation upon target engagement, and the formation of more stable immunological synapses [2], we selected higher initial CAR T-cell concentrations to more accurately reflect the enhanced therapeutic efficacy observed in clinical settings. As a result, our model implements initial CAR T-cell numbers ranging from 0 to 100 cells in the spatial region considered, corresponding to 2 to 10 times the initial effector cell densities used by Cooper et al. [41]. This range is consistent with clinical observations, where CAR T-cell doses can vary substantially depending on patient-specific factors and the characteristics of the CAR construct [42].

2.2. Transition rules and biological parameter choices

Throughout the simulations, the status of individual lattice cells undergoes dynamic changes based on a set of transition rules governing the behavior and interactions of cells within the system. At each iteration of the simulation, these rules are applied, driving the ongoing updates to cell states and shaping the overall progression of the model. The values of the different biological parameters used in these rules are listed in Table 1.

Temporal variables. In our simulation framework, each discrete time increment corresponds to one hour. For scenarios with sparse tumor cells, we allotted a total duration of 1200 h, reflecting a time span of 50 days. Simulations portraying tumor cells consolidated into a dense, clustered structure spanned 2160 h, corresponding to a time frame of 90 days.

Tumor cell proliferation. The proliferation parameter chosen was $\rho = 1/1000$ h^{-1} that corresponds to tumor doubling times over one month, thus describing fast-growing cancers are currently used only in late stages of the disease after standard treatments have failed. Thus, in current clinical settings CAR T-cells are used against aggressive advanced forms of the disease justifying our choice [14].

Lifespan and proliferation of CAR T-cells. Isolated CAR T-cells have a fixed lifespan (τ) which we estimated to be $\tau = 336$ h (two weeks) based on recent literature [43,44]. After the exhaustion of CAR T-cell, they are removed from the lattice of the automata since they do not play a significant role anymore.

CAR T — tumor cell interaction and killing kinetics. The T-cell/target cell interaction parameters were obtained from recent experimental works addressing the biological details of those processes [35,36]. CAR T-cells possess a cytotoxic load that triggers apoptosis in tumor cells. Initially, each CAR T-cell has the maximum possible cytotoxic load. Encountering a tumor cell induces the release of the CAR T-cell's cytotoxic load. After each hit, CAR T-cells require 8 h to fully replenish their cytotoxic load. Thus, throughout their lifespan, each CAR T-cell can execute a maximum of 42 cytotoxic hits. Nevertheless, it is plausible that during the simulation, some CAR T-cells may not come into contact with any tumor cells and, consequently, die without executing any targets.

Each tumor cell can be targeted by multiple CAR T-cells simultaneously or sequentially, leading to the accumulation of cytotoxic load of each contact. As the number of contacts increase, so does the likelihood of the tumor cell's demise, where the probability of death as a function of the number of contacts is denoted by α_n. A single CAR T-cell contact results in a 5% probability of cell death. However, with two CAR T-cells interacting simultaneously, the probability rises to 12%. For three or four CAR T-cells, the likelihood of target cell death reaches 50%. When a tumor cell is hit by five or six CAR T-cells simultaneously, the probability of death jumps to 80%. Finally, with seven or eight simultaneous targets, the probability of cell death peaks at 99% [35,36]. After a tumor cell dies it is removed instantaneously from the lattice.

CAR T-cell proliferation. After releasing the cytotoxic load upon hitting a target, CAR T-cells enter the duplication phase. During this stage, CAR T-cells remain stationary, neither moving nor targeting, as they prepare for duplication. After a 24-h period, the CAR T-cell divides into two: the original cell and a new CAR T-cell. The original cell retains its remaining lifespan, while the new CAR T-cell is born with 336 h of lifespan. Activated CAR T-cells have a maximum number of duplications, the so-called Hayflick limit [45,46], assumed to be 20 in this work and in line with biological evidence, although this number may depend on the patient's age and immunological status [47]. The new CAR T-cell inherits the duplication count from the original cell. For instance, if the original cell has undergone 15 duplications, the count will be 16 in the subsequent time interval for both cells. Upon reaching the maximum number of duplications, the CAR T-cell ceases to divide. We have also studied scenarios with duplication periods different from 24 h, with results listed in the Supplementary data.

Cell motility. Throughout the simulation, tumor cells remain static at predetermined locations, while CAR T-cells have the ability to move across the lattice. To implement this movement, we considered CAR T-cells to move randomly within their Moore neighborhoods once per time interval, in this case, one hour. Consequently, a CAR T-cell can move to one of the eight adjacent cells as long as they are unoccupied. CAR T-cells with no available space in their neighboorhood, remain in its current location.

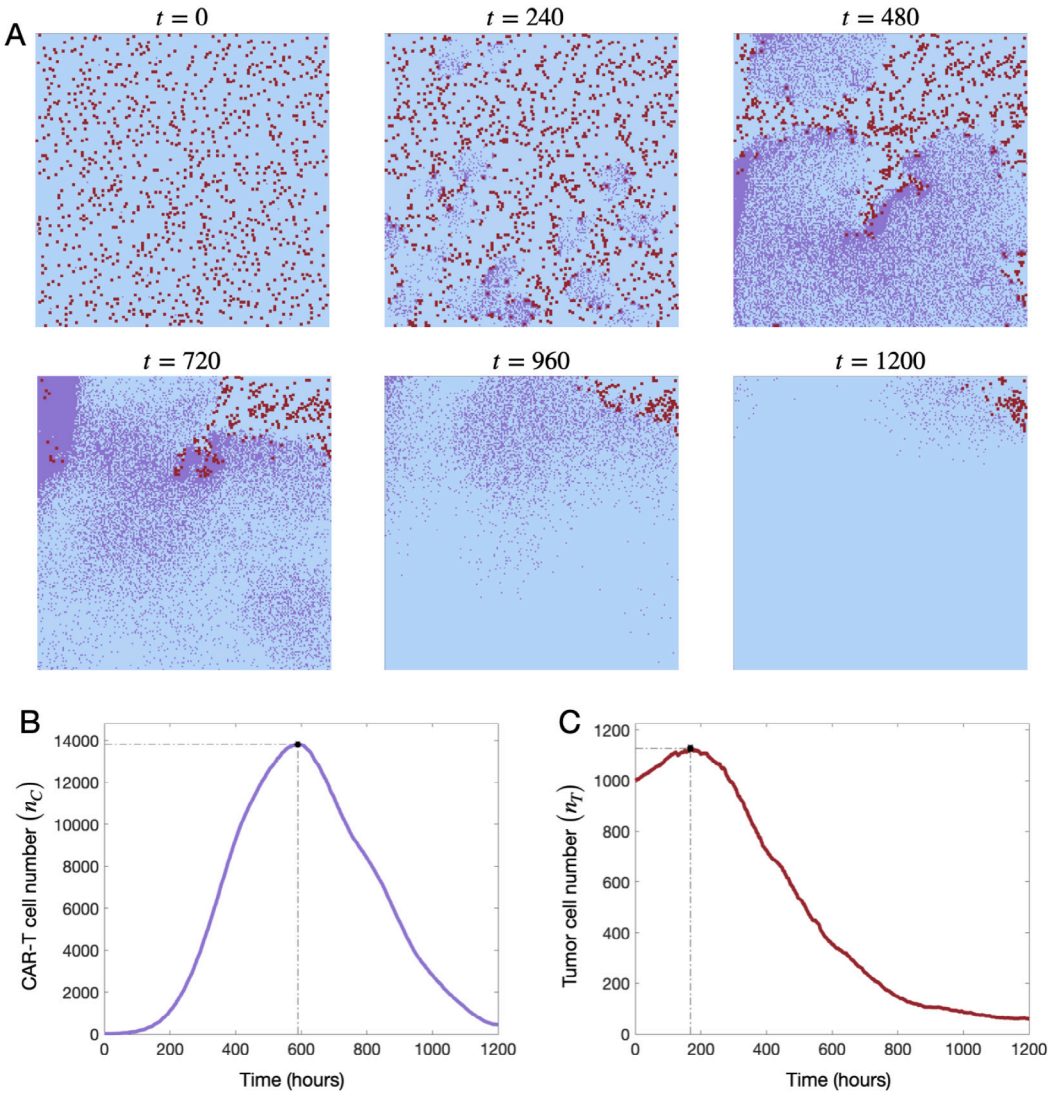

Fig. 2. Dynamics of CAR *T* and tumor cells proliferation with a sparse initial tumor cell distribution. (A) Representative images of tumor and CAR T-cell distribution at different timepoints (in hours) during the simulation. (B-C) Expansion kinetics of the CAR *T* (B) and tumor cell (C) populations. Starting cell numbers for this simulation were 1000 tumor cells and 20 CAR T-cells. CAR T-cells are shown in purple and tumor cells in red.

Table 1
Summary of biological parameter values used for the cellular automata.

Parameter	Value	Units	Source
ρ	1/1000	hours^{-1}	[14]
τ	336	hours	[43,44]
t_{charge}	8	hours	[35,36]
n_{dup}	20	dimensionless	[35,36]
t_{dup}	24	hours	[35,36]
α_n	0.05, if $n = 1$ 0.12, if $n = 2$ 0.50, if $n = 3,4$ 0.80, if $n = 5,6$ 0.99, if $n = 7,8$	dimensionless	[35,36]

2.3. Computational implementation

The model was implemented in MATLAB version: 9.12 (R2022a). To enhance the reliability of our analyses, we employed a fixed random seed across all simulations. This approach ensured reproducibility, as each rerun of the code produced identical initial cell arrangements. Such consistency facilitated not only the comparison of results but also the robust validation of the model's predictive capabilities. Further details regarding the code and visualization can be found in the Github repository https://github.com/sibordel/CellularAutomataCAR-T.git.

3. Results

3.1. Sparsely distributed tumor cells are more efficiently eliminated by CAR T-cells

To establish the dynamics of CAR T-cell-mediated killing we simulated a sparse distribution of tumor cells randomly located within the computational domain (Fig. 2(A)). In this analysis, the number of CAR T-cells is represented as n_C and the number of tumor cells as n_T with 1000 tumor cells and 20 CAR T-cells initially seeded. This translates to an effector (CAR T-cell) to target (tumor cell) ratio (ET ratio) of 1:100, reflecting a sparsely infiltrated tumor tissue.

Our simulation shows a strong expansion of the CAR T-cell population after encountering tumor cells (Fig. 2(B)). The increasing CAR T-cell numbers are accompanied by a decrease in the number of tumor cells over time (Fig. 2(C)), demonstrating the effectiveness of CAR T-cell therapy in targeting and eliminating sparsely distributed tumor cells. The number of tumor cells peaks at hour 168, just before

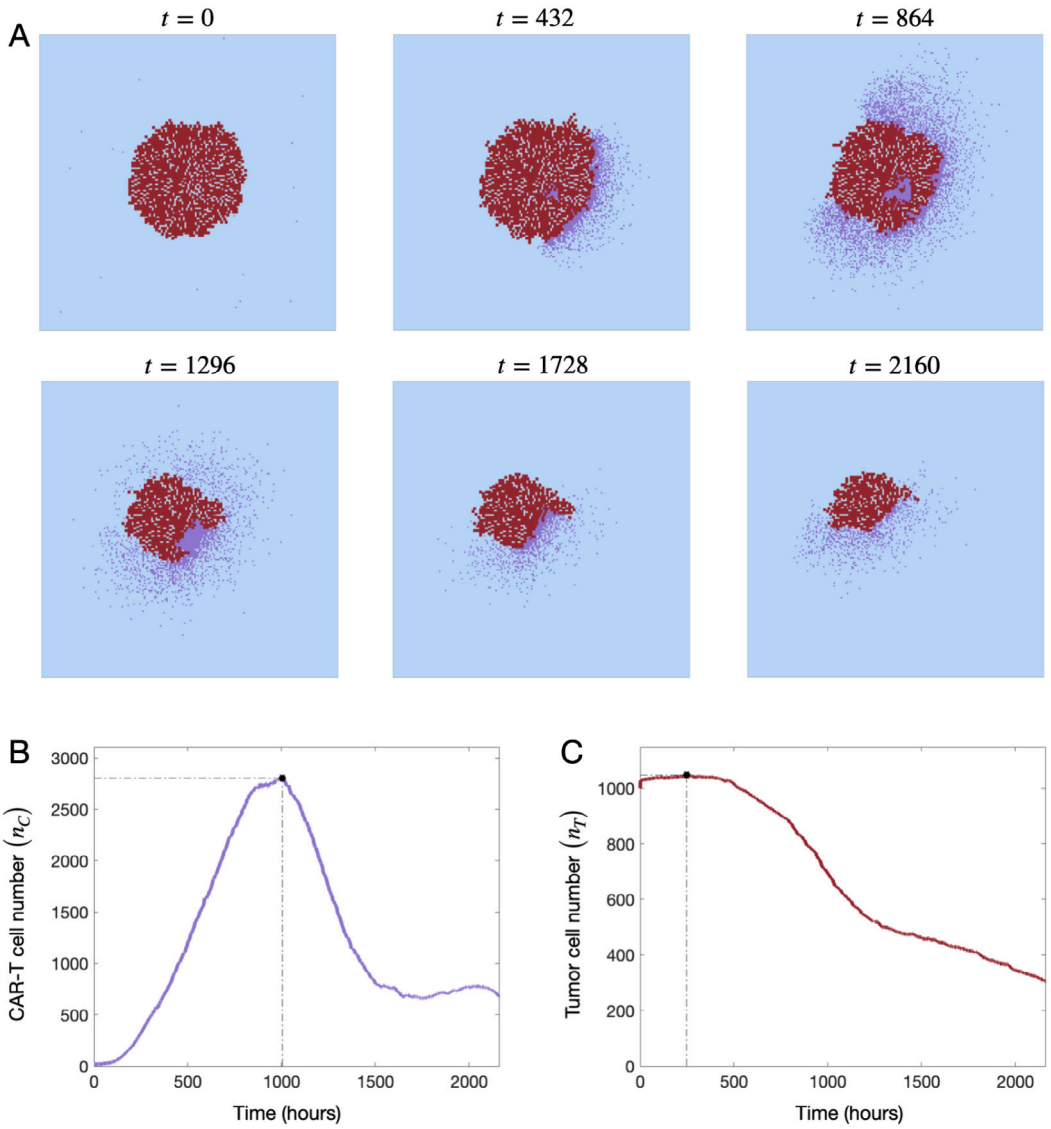

Fig. 3. Dynamics of CAR *T* and tumor cells with a dense and compact initial tumor cell distribution. (A) Representative images of tumor and CAR T-cell distribution at different timepoints (in hours) during the simulation. (B, C) Expansion kinetics of the CAR *T* (B) and tumor cell (C) populations. Starting cell numbers: 1000 tumor cells and 20 CAR T-cells. CAR T-cells are shown in purple and tumor cells in red.

initiating a robust decline, indicating the timepoint at which CAR T-cells reached a sufficient density to effectively target and eliminate the tumor cells. This correlated with an effector to target cell ratio (ET ratio) of approximately 1:15.

To address how the geometry of tumor cell positioning affects CAR T-cell-mediated killing of tumor cells, we proceeded to study a scenario where tumor cells were arranged in a cell-dense, compact solid tumor-like configuration (Fig. 3(A)). Similarly to the setup with sparse tumor cell distribution, we initially seeded 1000 tumor cells and 20 CAR T-cells. Tumor cells were arranged in a compact shape located at the center of the automata (Fig. 3(A)) and the simulations covered a period of 90 days (2160 h).

In this scenario, the dense clustering of tumor cells limited physical contacts between CAR T-cells and their targets to the tumor-tissue interface. Consequently, CAR T-cell expansion was significantly reduced, compared to the sparse tumor cell distribution. Specifically, the maximum CAR T-cell count peaked after 2805 h, significantly later compared to the simulation with sparse tumor cell distribution (after 1004 h). Correspondingly, the peak number of tumor cells was recorded at $t = 1048$ h, significantly later than in the sparse configuration where tumor cell numbers peaked at hour $t = 168$.

3.2. Insensitivity of model results to tumor proliferation rates

In our study, we assumed a constant proliferation rate of tumor cells. Previous research [11] explored a range of values for this rate ranging from 1/720 to 1/1440 h^{-1}. For most simulations in this paper we chose a rate of 1/1000 h^{-1}, roughly in the middle of this range. To address, whether this value accurately represented the system or if adjustments would affect our model's behavior we explored a broad range of ρ values for tumor cells distributed sparsely (Fig. 4) or as compact tumor mass (Fig. 5). In both settings, tumor cells were randomly distributed with a fixed number of initially seeded tumor and CAR T-cells. For sparsely distributed and clustered tumor cells, the evolution of cell populations over time showed comparable trends across all three ρ values. This suggests that the proliferation rate ρ may not have had a significant impact on model dynamics within the investigated parameter range. This relative insensitivity of the model to changes in ρ indicates a robustness in cellular dynamics against fluctuations in this parameter, observed for both sparse and compact tumor cell configurations.

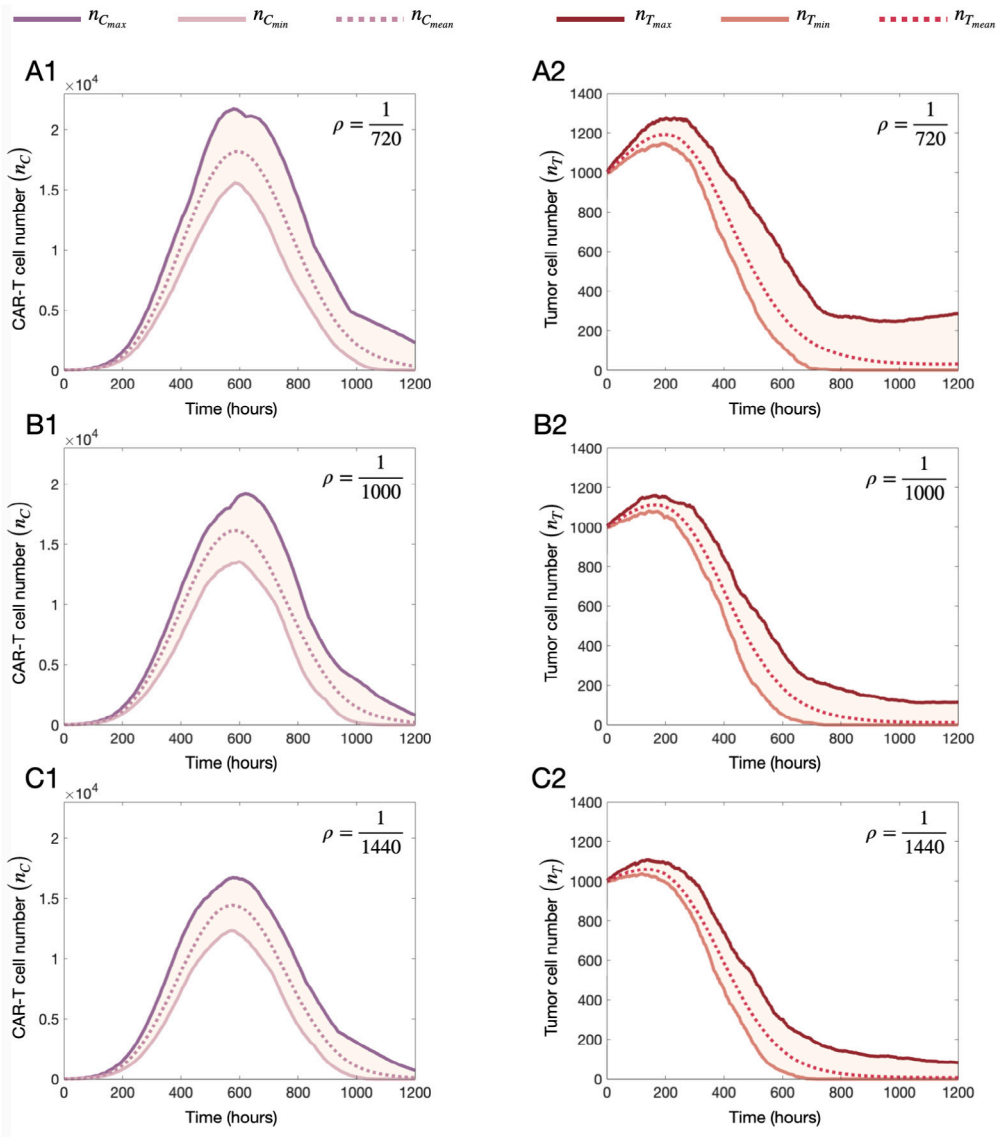

Fig. 4. Dynamics of sparse tumor cell configurations for different values of ρ. All simulations started with 1000 tumor and 20 CAR T-cells. One hundred different random seeds were simulated. The $n_{C_{max}}$ and $n_{T_{max}}$ curves represent the maximum value of CAR T-cells and tumor cells, at each time step of the simulation across the set of all simulations. $n_{C_{min}}$ and $n_{T_{min}}$ curves represent the minimum values of CAR T-cells and tumor cells at each time step. The $n_{C_{mean}}$ and $n_{T_{mean}}$ curves show the mean of all simulations. Panels display the behavior for different values of ρ. (A1, A2) $\rho = 1/720$ h^{-1}, (B1, B2) $\rho = 1/1000$ h^{-1}, (C1, C2) $\rho = 1/1440$ h^{-1}. CAR T-cell (A1, B1, C1) and tumor cell (A2, B2, C2) population dynamics are shown. Data from 100 simulations for each set of parameter values.

3.3. Dependence of treatment efficacy on CAR T-cell homing to the tumor

CAR T-cell numbers in the tumor depend on CAR T-cell proliferation in the TME and initial CAR T-cell extravasation from the blood vessels. We thus tested how the initial number of CAR T-cells present at the beginning of the simulation affects tumor immune control, simulating varying CAR T-cell extravasation rates in vivo. In these simulations, we fixed the initial tumor cell count to 600 and varied the number of CAR T-cells (10, 20 or 40 CAR T-cells). For both the sparse and compact tumor cell configurations, we conducted 100 simulations using different random seeds for each choice of cell numbers and configuration. The corresponding graphs for the cases of 800, 1000, 1200, and 1400 initial tumor cells can be found in the Supplementary data.

The simulations confirmed the previously observed differences in CAR T-cell expansion and tumor cell elimination in sparse (A1, B1, C1) and compact (A2, B2, C2) tumor cell configurations (Fig. 6). The maximum number of CAR T-cells was substantially higher when tumor cells were sparsely distributed, and the peak was reached earlier in the simulation. In simulations with compact tumor configurations, CAR T-cell numbers consistently remained close to zero, corresponding to a large fraction of simulations with minimal CAR T-cell expansion (Fig. 6, A2, B2, C2). However, comparing the maximum CAR T-cell numbers and the timepoints the peak was reached showed no significant differences between simulations starting with different CAR T-cells numbers. This indicates that the initial number of CAR T-cells has less impact on the maximum expansion compared to the CAR T-cell-intrinsic proliferation rate.

3.4. Initial tumor load determines peak CAR T expansion and initial number of cells injected influences time to peak

To quantify the relation between CAR T-cells initially present at the start of the simulation and the impact of tumor cell numbers on the timepoint of maximum CAR T-cell expansion, we plotted the maximum count of CAR T-cells (Fig. 7(A1, A2)) and the time when it occurred (Fig. 7(B1, B2)) in sparsely and clustered tumor cell distributions with

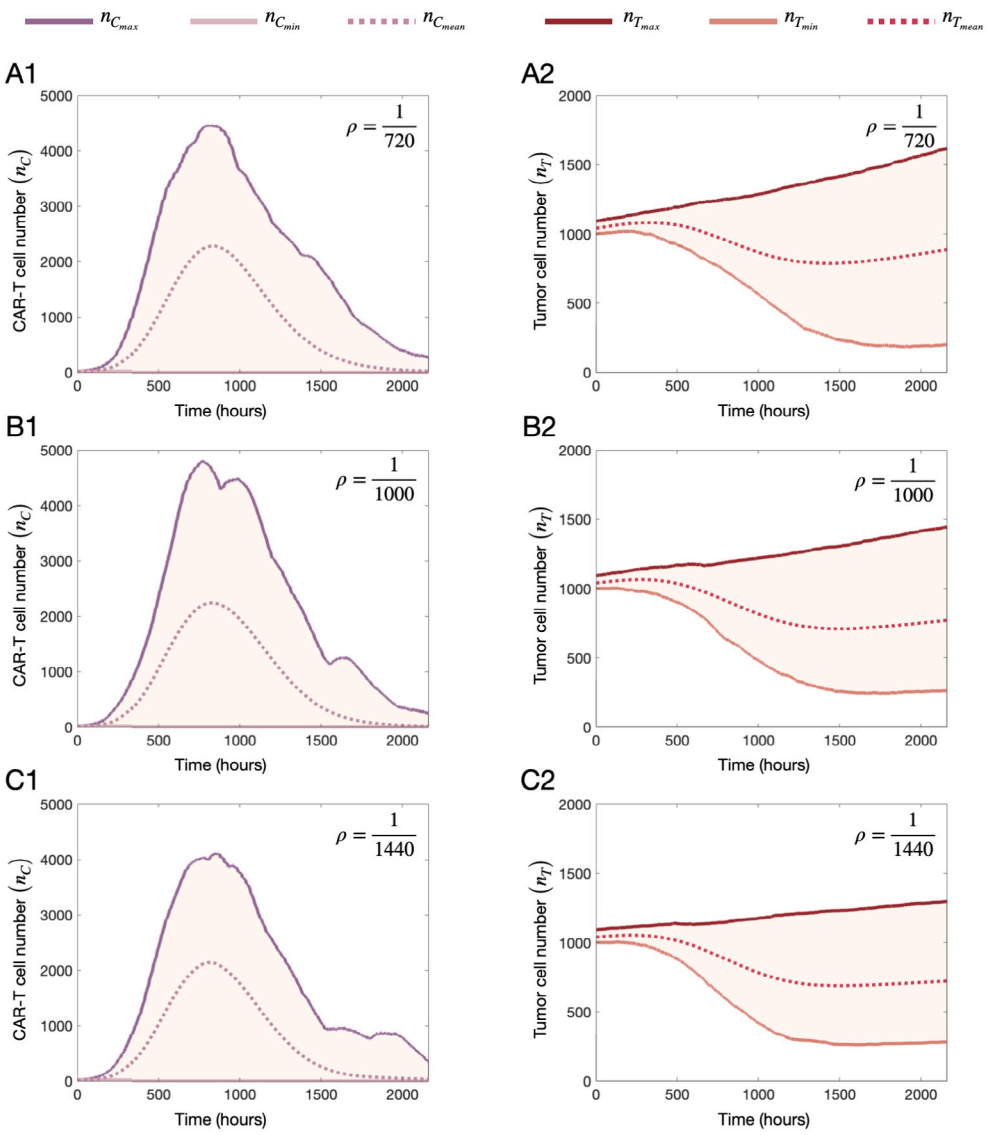

Fig. 5. Dynamics of compact tumor cell configurations for different values of ρ. All simulations started with 1000 tumor and 20 CAR T-cells. One hundred different random seeds were simulated. The $n_{C_{max}}$ and $n_{T_{max}}$ curves represent the maximum value of CAR T-cells and tumor cells, at each time step of the simulation across the set of all simulations. $n_{C_{min}}$ and $n_{T_{min}}$ curves represent the minimum values of CAR T-cells and tumor cells at each time step. The $n_{C_{mean}}$ and $n_{T_{mean}}$ curves show the mean of all simulations. Panels display the behavior for different values of ρ. (A1, A2) $\rho = 1/720$ h^{-1}, (B1, B2) $\rho = 1/1000$ h^{-1}, (C1, C2) $\rho = 1/1440$ h^{-1}. CAR T-cell (A1, B1, C1) and tumor cell (A2, B2, C2) population dynamics are shown. Data from 100 simulations for each set of parameter values.

increasing numbers of initial tumor cells. For each condition, we ran 100 independent simulations. From these, we extracted the highest number of CAR T-cells reached across all simulations and recorded the corresponding time in the simulation at which this maximum occurred. These values reflect the global peak expansion dynamics under each scenario and correspond to the variable $n_{c_{peak}}$ analyzed in Fig. 6 and Figures 3–6 of the Supplementary data.

For sparsely distributed tumor cells, we found that the maximum number of CAR T-cells increased depending on the number of tumor cells seeded at the beginning of the simulation (Fig. 7(A1)). While the peak number of CAR T-cells did not depend on the number of CAR T-cells seeded initially, the timing of its occurrence did (Fig. 7(B1)). We consistently observed an earlier occurrence of the maximum CAR T-cell expansion with increasing initial CAR T-cell numbers. The time required to reach the maximum CAR T-cell expansion was independent on the initial number of tumor cells in the range studied (Fig. 7(B1)). Consistently, in simulations with clustered tumor cells, the initial number of tumor cells influenced the maximum expansion of CAR T-cells (Fig. 7(A2)) and the initial number of CAR T-cells modulated the timepoint when the peak expansion was reached (Fig. 7(B2)), but both effects were weaker than in simulations with sparsely distributed tumor cells.

In summary, the initial number of tumor cells influenced the maximum expansion of CAR T-cells but not the time until the peak expansion was reached. In contrast, the initial number of CAR T-cells did not influence the maximum expansion of CAR T-cells but accelerated the time until the peak expansion was reached.

3.5. Initial states determine therapy success or failure

Finally, to comprehensively evaluate tumor response to CAR T-cell treatment at the end of the simulation for sparsely and clustered tumor cell distribution and the initial quantities of tumor and CAR T-cells, we applied extensive simulations (Fig. 8(A, B)). For each configuration and pair of values of the initial tumor and CAR T-cell numbers we run 20 simulations and classified the response for each choice of the initial number in either complete response (elimination of all cancer cells in all of the 20 simulations), no response (mean growth of tumor cells)

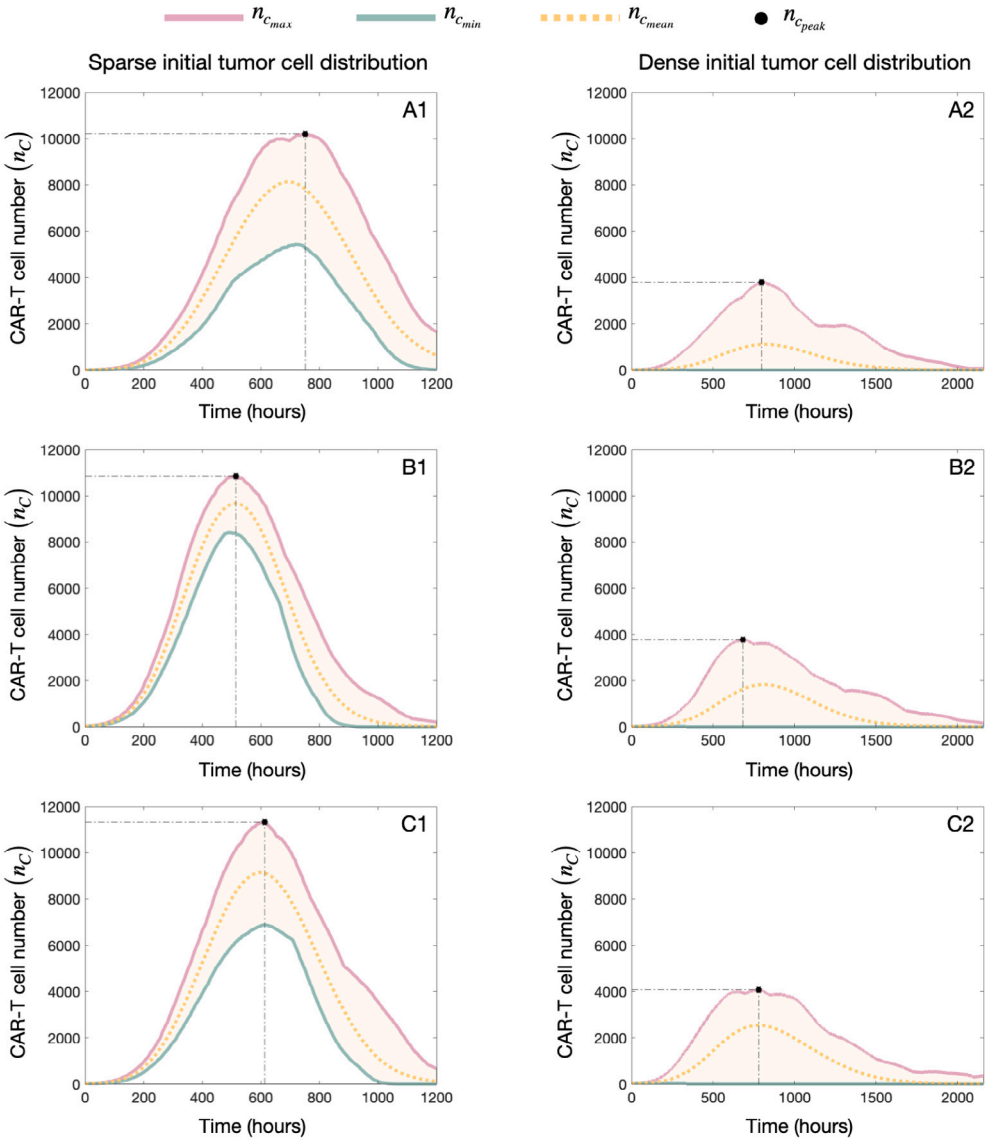

Fig. 6. Dynamics of CAR T-cell populations for n_T = 600 initial tumor cells and varying initial values of CAR T-cells. Pink, yellow and green lines represent respectively the maximum, average and minimum values obtained at each time step after conducting 100 simulations with different initial configurations. Results are shown for sparse (A1, B1, C1) or compact (A2, B2, C2) initial tumor cell configurations and 10 (A1, A2), 20 (B1, B2) or 40 (C1, C2) initial CAR T-cells. Data from 100 simulations for each set of parameter values. Supplementary data contains the corresponding graphs for the cases of 800, 1000, 1200, and 1400 initial tumor cells.

and different categories depending on whether the mean tumor cell number reduction at the end of the simulation was between 0%–25%, 25%–50%, 50%–75%, 75%–100%. A total of 33 different values of the initial tumor load and 100 values of the initial number of CAR T-cells where studied leading to a total of 66 000 simulations. We observed a full range of therapy response, ranging from complete tumor remission to immune evasion indicated by continued tumor growth (Fig. 8(A, B)).

The count of CAR T-cells increases incrementally from 1 to 100, while the number of tumor cells varies in increments of 25, ranging from 600 to 1400. Consequently, each graph comprises a total of 330 data points.

Complete tumor remission was observed with higher frequency in simulations where tumor cells were sparsely distributed, while complete remission was never observed in clustered tumor cells (Fig. 8(A, B)). Furthermore, in the case of sparse tumor configurations, treatment appears to be largely effective, as indicated by the scarcity of simulations resulting in overall tumor growth or response rates below 50% response rate (Fig. 8(A)). Conversely, in simulations starting with already clustered tumor cells, treatment efficacy is diminished, with minimal tumor reduction observed in the majority of cases (Fig. 8(B)). In both tumor geometries, efficacy was dependent on CAR T-cell numbers at the beginning of the simulation. Even sparsely distributed tumor cells could be controlled when less than 25 CAR T-cells were present at the beginning of the simulation, representing a starting ET ratio ranging from 1:24–1:56, depending on the number of tumor cells present. In contrast, 94% of the tumors were eradicated when the starting ET ratio ranged from 1:6–1:14. In compact tumors, no tumor decreased more than 50% at ET ratios ranging from 1:14–1:31 or lower while tumor response rates ranged between 75%–100% at ET ratios of 1:6–1:14. Interestingly there was a sustained trend in reduction of CAR T-cell effectiveness in compact tumors with increasing numbers of tumor cells which was not observed for sparsely distributed tumor cells (Fig. 8(A, B)). The perimeter to surface area decreases with increasing radius and thus indicates tumor size as a major determinant of treatment failure when CAR T-cells infiltrate the tumor from the tumor-tissue interfaces.

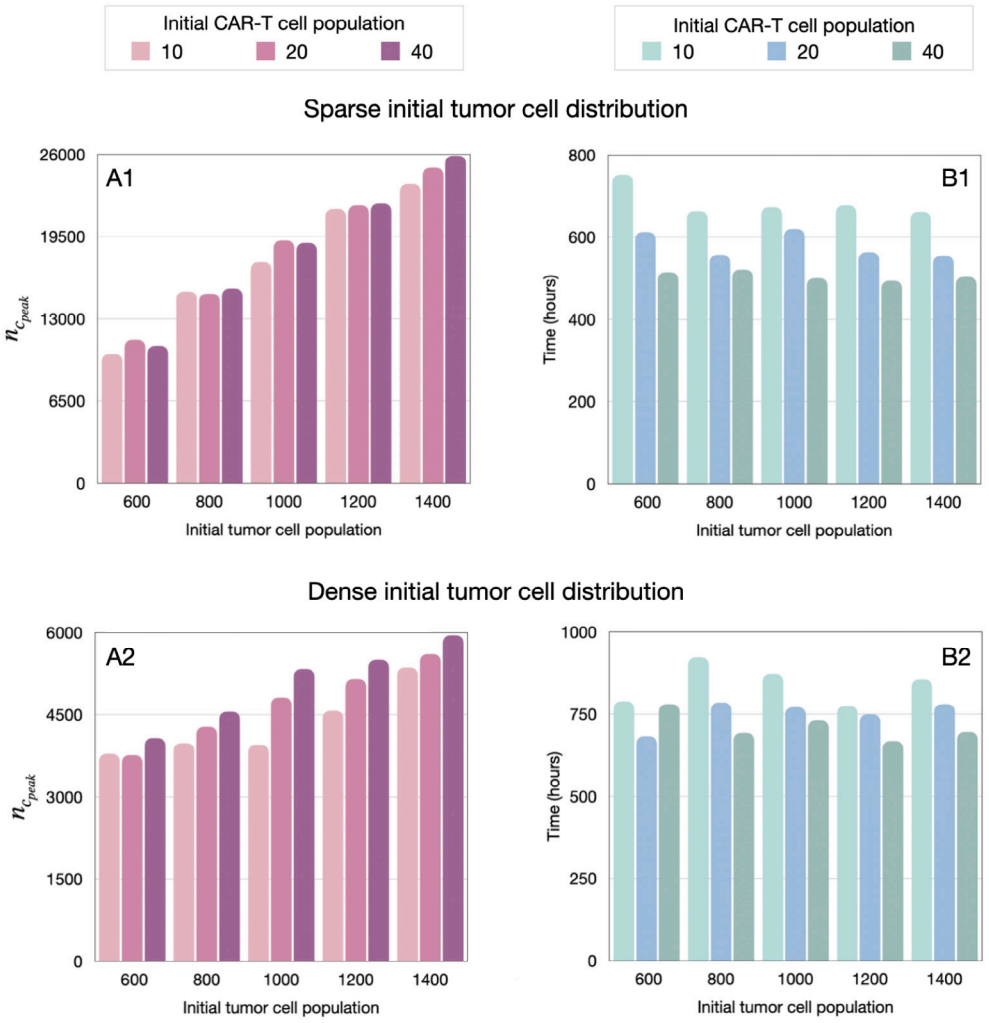

Fig. 7. Peak number and time of peak expansion of CAR T-cells in sparse and dense tumor cell configurations. (A1, A2) Maximum number of CAR T-cells obtained for different initial values of CAR *T* (10, 20, 40) and tumor cells (600, 800, 1000, 1200, 1400). (B1, B2) Time to peak CAR T-cell expansion for the numbers of CAR *T* and tumor cells. The exact values from the graph can be found in Supplementary data.

4. Discussion

The interest in mathematical descriptions of immunotherapy treatments for cancer, specifically targeting CAR T-cells, has been steadily growing. This trend reflects a recognized need to enhance our understanding of the intricate dynamics involved in immunotherapeutic approaches that involve in-patient expansion of the drug, exhaustion, phenotype changes between the different *T* lymphocytes injected and their competition with the target tumor cells and the off-tumor on target effects as well as treatment toxicity. Mathematical modeling provides a valuable tool for dissecting the complex interactions between effector cells and target cells, offering insights into treatment efficacy and suggesting potential optimization strategies. This study contributes to the ongoing efforts to leverage mathematical frameworks for advancing cancer immunotherapy research.

Most mathematical studies available up to now have focused on the global interactions between the effector and target cells by using compartmental differential equation models to describe CAR T-cell immunotherapy [10–18,48–54]. However, the interactions between T-lymphocytes and cancer cells require a direct physical interaction between both types of cells. This is why in this study we considered spatial aspects of the interactions using a cellular automata. This methodology enabled us to elucidate the nuanced cellular-level dynamics, yielding valuable insights into the mechanisms governing CAR T-cell therapy. Grounded in cellular automata, our modeling approach facilitated a comprehensive exploration of the spatial dimension in cellular dynamics. Unlike conventional models reliant on differential equations, do not account for spatial interactions, our method provided a more realistic depiction of cell distribution and organization within tumor tissue.

Consequently, here we intended to provide a complementary perspective in precisely evaluating the impact of tumor geometry on the effectiveness of CAR T-cell immunotherapy. Our focus was on studying how different tumor geometries could influence the effectiveness of CAR T-cell therapy, thus providing some sort of geometrical immune suppression mechanism that could add to others known to be present in solid tumors.

Our overarching objective was to enhance our understanding of the dynamics and outcomes associated with this treatment approach by investigating diverse scenarios encompassing varying initial counts of tumor cells and CAR T-cells. An important finding emerging from this research highlights the significant impact of tumor geometry on treatment effectiveness, revealing notable differences in responses between tumors characterized by compact cellular arrangements and those with sparse cells configurations. This disparity can be directly attributed to the increased frequency of interactions between tumor and CAR T-cells within sparse tumors. By fostering a higher initial contact density, sparse tumors facilitate greater opportunities for cell duplication, resulting in a more robust expansion of the CAR T-cell population compared to compact tumors. This observation not only aligns with clinical evidence showing better outcomes of CAR T-cell

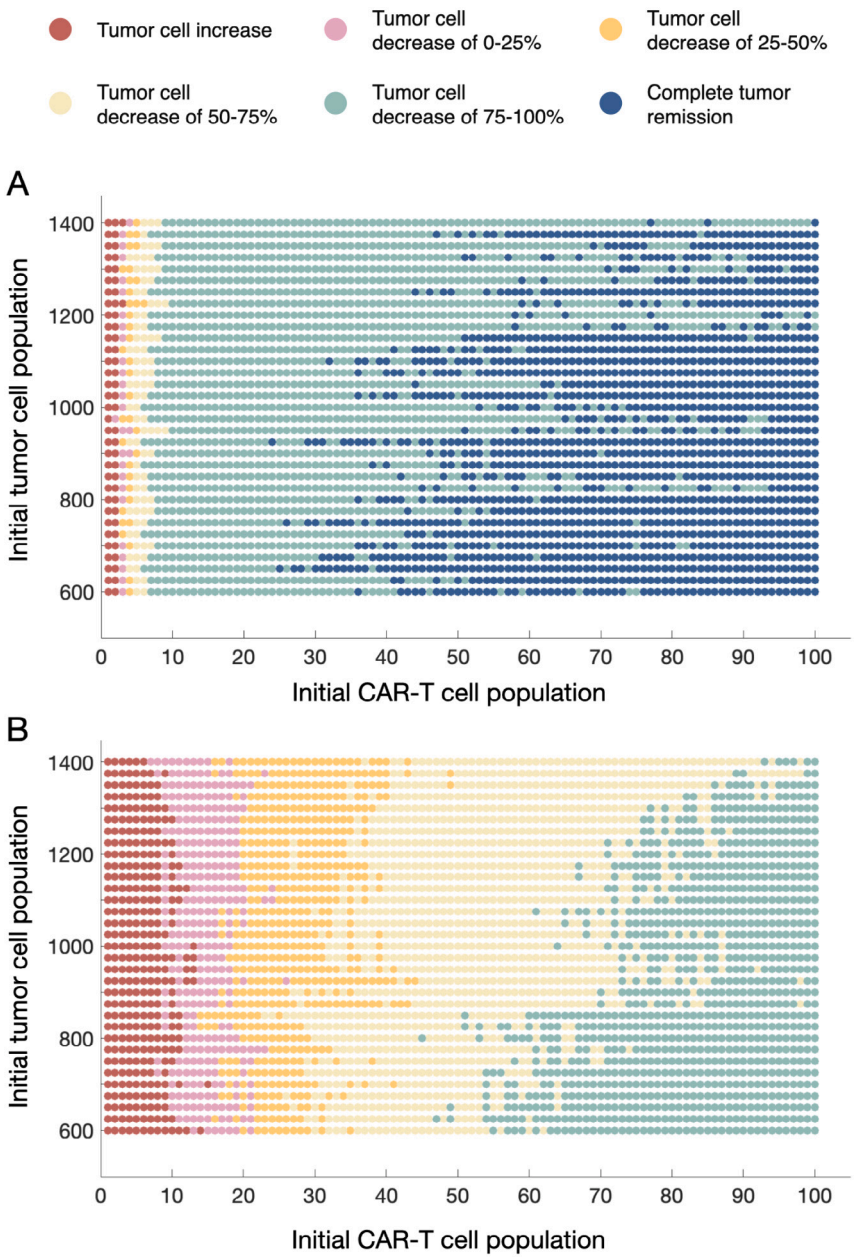

Fig. 8. Impact of the initial number of tumor cells, CAR T-cells, and tumor geometry on treatment outcome. Sparse (A) and compact (B) tumor geometries were explored. For each value of the tumor cell number in the range 600 to 1400 cells (Y axis) and CAR T-cell number in the range 1 to 100 (X axis) each point indicates the outcome of 20 simulations with different initial random seeds. Red indicate growth of the mean of the simulations in comparison with the initial number of tumor cells, pink denotes <25% reduction, orange represents 25%–50% reduction, yellow corresponds to 50%–75% reduction, green indicates >75% reduction, and blue denotes complete remission in all of the 20 simulations.

therapy in hematologic malignancies like leukemias, lymphomas, and myelomas [55,56] and highlights another effect that could limit the efficacy of these treatments on solid tumors. Despite ongoing advancements, effectively translating these therapeutic benefits to solid tumors remains a formidable challenge [57–59].

The initial spatial placement of CAR T-cells relative to tumor cells is a critical factor influencing their infiltration and subsequent engagement with the tumor mass. In our model, CAR T-cells are initially distributed randomly across the domain, reflecting the clinical practice of administering CAR T-cells via systemic infusion [2,60], which typically results in a relatively random localization within the patient's bloodstream. However, due to the absence of vascular structures in our current two-dimensional model, CAR T-cells cannot infiltrate the tumor mass, and this aspect is not considered in this version of the model. The infiltrative capacity of CAR T-cells in solid tumors is severely limited by the challenging tumor microenvironment. Upon reaching the tumor, CAR T-cells encounter significant obstacles, including an immunosuppressive environment, which hampers their ability to effectively penetrate the tumor core and engage with cancer cells. This ultimately hinders their therapeutic activity and allows tumor growth to persist [59,61]. As a result, in our model, the interactions between CAR T-cells and tumor cells are predominantly confined to the tumor periphery, leaving the interior of the tumor block largely intact.

Our observations highlight an interesting aspect regarding the initial population of CAR T-cells and its temporal impact on treatment dynamics. We noted that the initial number of CAR T-cells notably influences the time required to reach the peak CAR T-cell count in the system. This implies that the temporal dynamics of treatment are influenced by the number of injected cells. More precisely, we found that a larger initial population of CAR T-cells correlated with a shorter time to reach the

peak CAR T-cell count. It is remarkable that the inverse relationship between initial CAR T-cell numbers and time to peak arises as an emergent phenomenon of the model dynamics. This trend consistently appeared across all parameter combinations explored, regardless of specific values, indicating that it is not simply a result of particular parameter choices. Interestingly, this behavior has also been reported in simpler compartmental models [11], suggesting that it may be a general feature of CAR T-cell expansion dynamics. Even more relevant is the fact that there was a sustained trend in reduction of effectiveness of the treatment in compact tumors as the number of cancer cells increased that was not as evident in sparse tumors. It is clear that the perimeter to surface area decreases with the radius and thus lesion size would be a major determinant of treatment failure in compact solid tumors. Additionally, we observed that the timing of the CAR T population peak was also influenced by other model parameters. One important factor is the CAR T-cell duplication time (t_{dup}), which we set to 24 h in the main text. To explore the effect of this parameter, we performed additional simulations in the Supplementary data using t_{dup} values of 48 and 72 h. The results show that longer duplication times delay the peak of CAR T-cell expansion, highlighting the role of intrinsic proliferation kinetics in shaping treatment dynamics. Our CAR T-cell expansion is slower than that observed in the clinical setting, where peak expansion typically occurs around 1–2 weeks after infusion [62]. In our model, with the parameters used in the main text, peak expansion occurs around 24 days after infusion, although this timing may vary depending on the specific model parameters. This slower expansion is reasonable given that our model operates in a two-dimensional spatial context where there is less room for interactions and growth compared to three-dimensional environments.

The combination of CAR T-cells with treatments that make tumors more accessible to T-cells could be crucial for success. For example, radiopharmaceutical therapies (RPTs) could use the same surface molecule/antigen as the CAR product. Due to their different mechanisms of action, CAR T treatments could be more effective after RPTs, as the increased accessibility to internal tumor areas created by RPTs would render solid tumors more susceptible to CAR T-cells. High-risk localized prostate cancer has a high recurrence rate due to failed local control and micrometastatic disease. Lutetium PSMA, a radioligand targeting PSMA-expressing prostate cancer cells, has shown efficacy in metastatic castration-resistant prostate cancer. Combining lutetium PSMA with systemic immunotherapies could enhance the anti-tumor T-cell response, potentially improving long-term immunity and targeting occult micrometastases [63].

However, it is essential to acknowledge the limitations inherent in our study. The cellular automata model we utilized represents only a small fraction of the tissue, specifically 4 mm^2. It could be relevant to extend the model to a larger scale, encompassing broader tissue areas, including vessels and other elements of the tumor microenvironment. Transitioning to a larger scale would permit a more thorough assessment of how cellular processes and tissue interactions manifest at a macroscopic level. Furthermore, given that our current cellular automata model operates within a two-dimensional domain, it is important to acknowledge that this approach, while valuable, does not fully capture the three-dimensional complexity observed in actual tumor tissues. Tumors exist in a highly intricate three-dimensional microenvironment where spatial interactions, diffusion dynamics, and cell-to-cell communication occur in a manner that cannot be entirely replicated in a two-dimensional framework. Consequently, future research should focus on extending the model into three dimensions to better reflect these biological realities. Implementing a three-dimensional cellular automata model would allow for a more accurate representation of tumor morphology, heterogeneity, and the spatial distribution of CAR T-cells within the tumor mass. This advancement could provide deeper insights into treatment dynamics, ultimately enhancing the clinical relevance and predictive power of our modeling approach. These deliberations underscore the importance of ongoing exploration and refinement of our modeling methodologies to achieve a more holistic and precise representation of biological systems in the context of CAR T-cell therapy.

Our study addresses treatment of a late stage cancer, that in general tend to be invasive and more migratory than early stage ones. One may wonder if the lack of movement of cancer cells in the model would adequately reflect the biology and if allowing cancer cells to move could change the results. This is an interesting question for which additional computational work could be developed. Our focus was to investigate spatial interactions between CAR T-cells and tumor cells within a static environment. Although late-stage cancers are often more invasive, our model did not include cancer cell migration due to the lack of details of several aspects affecting cancer cell motility including tissue structures, such as extracellular matrix or vasculature, which is essential for tumor invasion, that are beyond the scope of this study. Nonetheless, we believe our conclusions would remain valid, particularly for solid epithelial tumors where the bulk tumor mass is largely immobile, and spatial organization primarily governs treatment dynamics. Sparse tumors, would allow for tumor cell movement that it is not likely to affect the outcome significantly, as CAR T-cell expansion ensures sufficient interactions regardless of target cell mobility. While future versions of the model may include migration, the static approach used here could be appropriate for addressing the question of how tumor geometry influences CAR T-cell efficacy.

In our model, the probabilities governing tumor cell death were based on experimental work by Weigelin et al. [35,36], which support an additive cytotoxicity mechanism. Those studies show that a single T cell contact rarely induces immediate apoptosis, but that the likelihood of tumor cell death increases cumulatively with each additional contact. Accordingly, our model incorporates a progressive killing probability — from 5% for a single contact to over 80% with multiple interactions — consistent with these findings. Other authors such as Korrel et al. [64] based on results originally reported by Cazaux et al. [65], have found that approximately 70% of tumor cell apoptosis results from direct CAR T-cell killing, where a single CAR T-cell interacts with one tumor cell. This discrepancy suggests that there may be a differences on this aspect of the CAR T-cell-tumor cell killing kinetics depending on many factors that could include the specific CAR T product, nature of the antigen and its expression level, level of exhaustion, etc. This leaves a door open for further explorations that may have an impact of the outcome of the treatments.

Activated CAR T-cells engaging tumor cells release cytokines that have a chemotactic effect on other CAR T-cells that result in their motion towards the tumor mass. In an earlier version of our study we implemented some rules to describe this phenomenon that did not change the qualitative dynamics in what concerns the role of the tumor morphology, that is the goal of this research. A proper fitting of those chemotactic phenomena requires identifying many additional parameters related to the chemoattractant secretion, diffusivity, response of the CAR T-cells to the chemical, duration of the response, etc., we opted for removing this mechanism from the model. However, this is a very interesting phenomenons that deserves further attention and would correspond a natural extension of our model presented here.

In our modeling approach, we simplified our representation by assuming that tumor cells do not experience changes over time. This simplification does not capture the full dynamic complexity of tumors, where genetic mutations and phenotypic heterogeneity are known to occur, although probably on longer timescales. Such mutations can lead to the emergence of therapy-resistant cell phenotypes, posing challenges to treatment efficacy. Moreover, tumors can develop immune evasion mechanisms, such as upregulation of immune checkpoint pathways, which may suppress CAR T-cell activity and limit therapeutic success. This phenomenon, commonly referred to as tumor escape, underscores the importance of considering the dynamic evolution of tumor cells in therapeutic strategies. In our model, we also assume that all tumor cells express the specific antigen targeted by CAR T-cells. Since no genetic mutation or antigen-loss mechanism is

implemented, antigen expression remains homogeneous throughout the tumor population. This simplification allows us to focus on spatial dynamics, but it does not capture the possibility of immune escape due to antigen loss variants. The study of the dynamics of antigen loss and emergence of resistant subpopulations during CAR T-cell treatments is a very relevant problem that could also be addressed with cellular automata. Incorporating tumor heterogeneity, genetic variability, and immune evasion mechanisms into simulation models could provide a more comprehensive understanding of disease dynamics and enable the development of more effective CAR T-cell therapies capable of overcoming resistance and improving treatment outcomes.

Recent advancements in CAR T-cell engineering have introduced strategies to enhance efficacy against solid tumors. One such approach involves armored CAR T-cells, which are genetically modified to secrete cytokines or express cytokine receptors, thereby modulating the tumor microenvironment to overcome immunosuppressive barriers. For instance, CAR T-cells engineered to secrete IL-12 have demonstrated improved antitumor activity in preclinical models by enhancing the immune response within the tumor environment [66,67].

Another promising strategy is the development of bispecific CAR T-cells, designed to target multiple tumor-associated antigens simultaneously. This dual-targeting capability addresses tumor heterogeneity and reduces the likelihood of antigen escape, a common challenge in solid tumor treatment. Studies have shown that bispecific CAR T-cells targeting antigens such as FAP and GPC3 can effectively control heterogeneous hepatocellular carcinoma in preclinical models [68].

5. Conclusion

In summary, our study highlights the relevance of considering spatial aspects when describing CAR T-cell immunotherapy mathematically. We have found a key role of the tumor geometry indicating a mechanism of 'geometrical' immune suppression based on the accessibility of tumor cells to infiltrating immune cells. We have also highlighted the relevant effect of tumor size and number of CAR T-cells homing to the tumor for the control of compact tumors, but not on sparse tumors that are easy to access for the curative effector cells. Moving forward, continued refinement and validation of cellular automata models will be essential to fully harness their potential and facilitate the development of more effective CAR T-cell therapies.

CRediT authorship contribution statement

Silvia Bordel-Vozmediano: Writing – review & editing, Writing – original draft, Visualization, Software, Methodology, Investigation, Formal analysis, Conceptualization. **Soukaina Sabir:** Writing – review & editing, Writing – original draft, Methodology, Investigation. **Lucía Benito-Barca:** Writing – review & editing, Software, Investigation. **Bettina Weigelin:** Writing – review & editing, Investigation. **Víctor M. Pérez-García:** Writing – review & editing, Supervision, Project administration, Methodology, Funding acquisition, Conceptualization.

Declaration of competing interest

The authors declare that there are no conflicts of interest regarding the publication of this article.

Acknowledgments

This work has been partially supported by project PID2022-142341OB-I00, funded by Ministerio de Ciencia e Innovación/Agencia Estatal de Investigación. Spain (doi:10.13039/501100011033) and European Regional Development Fund (ERDF A way of making Europe); grant SBPLY/21/180501/000145 (Junta de Comunidades de Castilla-La Mancha, Spain) and grant 2022-GRIN-34405 funded by University of Castilla-La Mancha/FEDER (Applied Science Projects within the UCLM research programme).

Appendix A. Supplementary data

Supplementary material related to this article can be found online at https://doi.org/10.1016/j.compbiomed.2025.110427.

Data availability

All relevant data are within the manuscript. The cellular automata code is available at https://github.com/sibordel/CellularAutomataCAR-T.git.

References

[1] A.D. Waldman, J.M. Fritz, M.J. Lenardo, A guide to cancer immunotherapy: from T cell basic science to clinical practice, Nat. Rev. Immunol. 20 (2020) 651–668, http://dx.doi.org/10.1038/s41577-020-0306-5.

[2] C.H. June, R.S. O'Connor, O.U. Kawalekar, S. Ghassemi, M.C. Milone, CAR-T cell immunotherapy for human cancer, Science 359 (6382) (2018) 1361–1365, http://dx.doi.org/10.1126/science.aar6711.

[3] R.C. Sterner, R.M. Sterner, CAR-T cell therapy: current limitations and potential strategies, Blood Cancer J. 11 (2021) 69, http://dx.doi.org/10.1038/s41408-021-00459-7.

[4] X. Zhang, L. Zhu, H. Zhang, S. Chen, Y. Xiao, CAR-T cell therapy in hematological malignancies: Current opportunities and challenges, Front. Immunol. 13 (2022) 927153, http://dx.doi.org/10.3389/fimmu.2022.927153.

[5] J. Lu, G. Jiang, The journey of CAR-T therapy in hematological malignancies, Mol. Cancer 21 (2022) 194, http://dx.doi.org/10.1186/s12943-022-01663-0.

[6] U. Uslu, C.H. June, Beyond the blood: expanding CAR-T cell therapy to solid tumors, Nature Biotechnol. (2024) 1–10, http://dx.doi.org/10.1038/s41587-024-02446-2.

[7] S.M. Albelda, CAR-T cell therapy for patients with solid tumours: key lessons to learn and unlearn, Nat. Rev. Clin. Oncol. 21 (1) (2024) 47–66, http://dx.doi.org/10.1038/s41571-023-00832-4.

[8] G. Guzman, M.R. Reed, K. Bielamowicz, B. Koss, A. Rodriguez, CAR-T therapies in solid tumors: opportunities and challenges, Curr. Oncol. Rep. 25 (5) (2023) 479–489, http://dx.doi.org/10.1007/s11912-023-01380-x.

[9] A. Schmidts, M.V. Maus, Making CAR T cells a solid option for solid tumors, Front. Immunol. 9 (2018) 2593, http://dx.doi.org/10.3389/fimmu.2018.02593.

[10] L. Liu, C. Ma, Z. Zhang, et al., Computational model of CAR-T-cell immunotherapy dissects and predicts leukemia patient responses at remission, resistance, and relapse, J. Immunother. Cancer 10 (12) (2022) http://dx.doi.org/10.1136/jitc-2022-005360.

[11] O. León-Triana, S. Sabir, G.F. Calvo, et al., CAR-T cell therapy in B-cell acute lymphoblastic leukaemia: Insights from mathematical models, Commun. Nonlinear Sci. Numer. Simul. 94 (2021) 105570, http://dx.doi.org/10.1016/j.cnsns.2020.105570.

[12] Á. Martínez-Rubio, S. Chulián, C. Blázquez Goñi, et al., A mathematical description of the bone marrow dynamics during CAR-T-cell therapy in B-cell childhood acute lymphoblastic leukemia, Int. J. Mol. Sci. 22 (12) (2021) 6371, http://dx.doi.org/10.3390/ijms22126371.

[13] R. Mostolizadeh, Z. Afsharnezhad, A. Marciniak-Czochra, Mathematical model of chimeric anti-gene receptor (CAR) T cell therapy with presence of cytokine, Numer. Algebra Control. Optim. 8 (1) (2018) 63–80, http://dx.doi.org/10.3934/naco.2018004.

[14] V.M. Pérez-García, O. León-Triana, M. Rosa, A. Pérez-Martínez, CAR-T cells for T-cell leukemias: Insights from mathematical models, Commun. Nonlinear Sci. Numer. Simul. 96 (2021) 105684, http://dx.doi.org/10.1016/j.cnsns.2020.105684.

[15] K. Roesch, D. Hasenclever, M. Scholz, Modelling lymphoma therapy and outcome, Bull. Math. Biol. 76 (2) (2013) 401–430, http://dx.doi.org/10.1007/s11538-013-9925-3.

[16] L.R.C. Barros, E.A. Paixão, A.M.P. Valli, G.T. Naozuka, A.C. Fassoni, R.C. Almeida, CARTmath—a mathematical model of CAR-T immunotherapy in preclinical studies of hematological cancers, Cancers 13 (12) (2021) 2941, http://dx.doi.org/10.3390/cancers13122941.

[17] K. Owens, I. Bozic, Modeling CAR-T-cell therapy with patient preconditioning, Bull. Math. Biol. 83 (5) (2021) http://dx.doi.org/10.1007/s11538-021-00869-5.

[18] G.J. Kimmel, F.L. Locke, P.M. Altrock, The roles of T cell competition and stochastic extinction events in chimeric antigen receptor t cell therapy, Proc. R. Soc. B 288 (1947) (2021) http://dx.doi.org/10.1098/rspb.2021.0229.

[19] O. León-Triana, A. Pérez-Martínez, M. Ramírez-Orellana, V.M. Pérez-García, Dual-target CAR-Ts with on- and off-tumour activity may override immune suppression in solid cancers: A mathematical proof of concept, Cancers 13 (4) (2021) 703, http://dx.doi.org/10.3390/cancers13040703.

[20] R. Li, P. Sahoo, D. Wang, D. Saha, A. Sharma, X. Zhang, Modeling interaction of glioma cells and CAR-T-cells considering multiple CAR-T-cells bindings, ImmunoInformatics 9 (2023) 100022, http://dx.doi.org/10.1016/j.immuno.2023.100022.

[21] M. Bodnar, U. Foryś, M.J. Piotrowska, M. Bodzioch, J.A. Romero-Rosales, J. Belmonte-Beitia, On the analysis of a mathematical model of CAR-T cell therapy for glioblastoma: Insights from a mathematical model, Int. J. Appl. Math. Comput. Sci. (2023) http://dx.doi.org/10.34768/amcs-2023-0027.

[22] P. Sahoo, X. Yang, D. Abler, A. Sandler, X. Wang, J. Lee, T. Zhang, M. Tan, Y. Yu, S. Ma, J. Lee, Y. Lin, C. Chen, S. Soni, P. Thall, S. Johnson, Mathematical deconvolution of CAR T-cell proliferation and exhaustion from real-time killing assay data, J. R. Soc. Interface 17 (163) (2020) 20190734, http://dx.doi.org/10.1098/rsif.2019.0734.

[23] K. Owens, A. Rahman, Bozic, Spatiotemporal dynamics of tumor - CAR T-cell interaction following local administration in solid cancers, 2024, http://dx.doi.org/10.1101/2024.08.29.610392, bioRxiv.

[24] J. von Neumann, A.W. Burks, et al., Theory of self-reproducing automata, 1966.

[25] A.W. Burks, Essays on Cellular Automata, University of Illinois Press, 1968.

[26] P. Gerlee, A.R.A. Anderson, An evolutionary hybrid cellular automaton model of solid tumour growth, J. Theoret. Biol. 246 (4) (2007) 583–603, http://dx.doi.org/10.1016/j.jtbi.2007.01.027.

[27] N. Kazmi, M.A. Hossain, R.M. Phillips, A hybrid cellular automaton model of solid tumor growth and bioreductive drug transport, IEEE/ACM Trans. Comput. Biol. Bioinform. 9 (6) (2012) 1595–1606, http://dx.doi.org/10.1109/TCBB.2012.118.

[28] H.M. Byrne, Dissecting cancer through mathematics: from the cell to the animal model, Nat. Rev. Cancer 10 (3) (2010) 221–230, http://dx.doi.org/10.1038/nrc2808.

[29] D.G. Mallet, L.G. De Pillis, A cellular automata model of tumor–immune system interactions, J. Theoret. Biol. 239 (3) (2006) 334–350, http://dx.doi.org/10.1016/j.jtbi.2005.08.002.

[30] S. Shahmoradi, F.N. Rahatabad, K. Maghooli, A stochastic cellular automata model of growth of avascular tumor with immune response and immunotherapy, Inform. Med. Unlocked 12 (2018) 81–87, http://dx.doi.org/10.1016/j.imu.2018.06.008.

[31] D. Bhavsar, Y.J. Li, Simulation-based software modeling of CAR T cell therapy efficacy against solid malignant tumors, Can. J. Med. 5 (1) (2023) 24–34, http://dx.doi.org/10.33844/cjm.2023.6029.

[32] A.N. Prybutok, J.S. Yu, J.N. Leonard, N. Bagheri, Mapping CAR T-cell design space using agent-based models, Front. Mol. Biosci. 9 (2022) 849363, http://dx.doi.org/10.3389/fmolb.2022.849363.

[33] H. Fischel, T. Giorgadze, A. Tessier, K.A. Norton, Computational modeling of chimeric antigen receptor (CAR) T-cell therapy of a binary model of antigen receptors in breast cancer, in: 2021 IEEE International Conference on Bioinformatics and Biomedicine, BIBM, IEEE, 2021, pp. 3267–3274, http://dx.doi.org/10.1109/BIBM52615.2021.9669393.

[34] S. Zouhri, S. Saadi, M. Rachik, Simulation of tumor response to immunotherapy using a hybrid cellular automata model, Int. J. Appl. Comput. Math. 3 (2) (2016) 1077–1101, http://dx.doi.org/10.1007/s40819-016-0163-x.

[35] B. Weigelin, A.T. den Boer, E. Wagena, L. Wassink, D. Oosterhoff, S. Weigelin, T. Zabeu, P. Sniatecki, R.J. de Boer, J. Fiedler, Cytotoxic T cells are able to efficiently eliminate cancer cells by additive cytotoxicity, Nat. Commun. 12 (1) (2021) http://dx.doi.org/10.1038/s41467-021-25282-3.

[36] B. Weigelin, P. Friedl, T cell-mediated additive cytotoxicity – death by multiple bullets, Trends Cancer 8 (12) (2022) 980–987, http://dx.doi.org/10.1016/j.trecan.2022.07.007.

[37] M.R. Benmebarek, C.H. Karches, B.L. Cadilha, S. Lesch, S. Endres, S. Kobold, Killing mechanisms of chimeric antigen receptor (CAR) T cells, Int. J. Mol. Sci. 20 (6) (2019) 1283, http://dx.doi.org/10.3390/ijms20061283.

[38] X. Jiang, S. Dudzinski, K.E. Beckermann, et al., MRI of tumor T cell infiltration in response to checkpoint inhibitor therapy, J. ImmunoTherapy Cancer 8 (2020) e000328, http://dx.doi.org/10.1136/jitc-2019-000328.

[39] Y.C. Ma, L. Wang, F.L. Yu, Recent advances and prospects in the isolation by size of epithelial tumor cells (ISET) methodology, Technol. Cancer Res. Treat. 12 (4) (2013) 295–309, http://dx.doi.org/10.7785/tcrt.2012.500328.

[40] R.E. Waugh, E. Lomakina, A. Amitrano, M. Kim, Activation effects on the physical characteristics of T lymphocytes, Front. Bioeng. Biotechnol. 11 (2023) 1175570, http://dx.doi.org/10.3389/fbioe.2023.1175570.

[41] A.K. Cooper, P.S. Kim, A cellular automata and a partial differential equation model of tumor–immune dynamics and chemotaxis, in: Mathematical Models of Tumor-Immune System Dynamics, Springer, 2014, pp. 21–46, http://dx.doi.org/10.1007/978-1-4939-1793-8_2.

[42] C.J. Turtle, L.A. Hanafi, C. Berger, T.A. Gooley, S. Cherian, M. Hudecek, D.G. Maloney, CD19 CAR–T cells of defined CD4+: CD8+ composition in adult B cell ALL patients, J. Clin. Investig. 126 (6) (2016) 2123–2138, http://dx.doi.org/10.1172/JCI85309.

[43] S. Ghorashian, A.M. Kramer, S. Onuoha, M. Doussau, M. Khalil, M. Khan, C. McCabe, M. McKendrick, R. Pepple, L. Harker, P. Zandstra, P. Xue, G. Wei, Enhanced CAR T cell expansion and prolonged persistence in pediatric patients with ALL treated with a low-affinity CD19 CAR, Nature Med. 25 (2019) 1408–1414, http://dx.doi.org/10.1038/s41591-019-0549-5.

[44] J. Westera, J. Drylewicz, I. den Braber, T. Mugwagwa, I. van der Maas, L. Kwast, T. Volman, E.H. van de Weg-Schrijver, I. Bartha, G. Spierenburg, K. Gaiser, M.T. Ackermans, B. Asquith, R.J. de Boer, K. Tesselaar, J.A. Borghans, Closing the gap between T-cell life span estimates from stable isotope-labeling studies in mice and humans, Blood 122 (13) (2013) 2205–2212, http://dx.doi.org/10.1182/blood-2013-03-488411.

[45] L. Hayflick, P.S. Moorhead, The serial cultivation of human diploid cell strains, Exp. Cell Res. 25 (3) (1961) 585–621, http://dx.doi.org/10.1016/0014-4827(61)90192-6.

[46] J.H. Noll, B.L. Levine, C.H. June, J.A. Fraietta, Beyond youth: Understanding CAR T cell fitness in the context of immunological aging, Sem. Immunol. 70 (2023) 101840, http://dx.doi.org/10.1016/j.smim.2023.101840.

[47] W. Ndifon, J. Dushoff, The Hayflick limit may determine the effective clonal diversity of naive T cells, J. Immunol. 196 (12) (2016) 4999–5004, http://dx.doi.org/10.4049/jimmunol.1502343.

[48] G.J. Kimmel, F.L. Locke, P.M. Altrock, Response to CAR-T cell therapy can be explained by ecological cell dynamics and stochastic extinction events, 2019, http://dx.doi.org/10.1101/717074, Cold Spring Harbor Laboratory.

[49] L.R.C. Barros, B. de Jesus Rodrigues, R.C. Almeida, CAR-T cell goes on a mathematical model, J. Cell Immunol. 2 (1) (2020) 31–37, http://dx.doi.org/10.33696/immunology.2.016.

[50] B. de Jesus Rodrigues, L.R.C. Barros, R.C. Almeida, Three-compartment model of CAR T-cell immunotherapy, 2019, 779793, http://dx.doi.org/10.1101/779793, bioRxiv.

[51] G.E. Mahlbacher, K.C. Reihmer, H.B. Frieboes, Mathematical modeling of tumor-immune cell interactions, J. Theoret. Biol. 469 (2019) 47–60, http://dx.doi.org/10.1016/j.jtbi.2019.03.002.

[52] C. Schacht, A. Meade, H.T. Banks, H. Enderling, D. Abate-Daga, Estimation of probability distributions of parameters using aggregate population data: analysis of a CAR-T cell cancer model, Math. Biosci. Eng. 16 (6) (2019) 7299–7326, http://dx.doi.org/10.3934/mbe.2019365.

[53] A.P. Singh, X. Zheng, X. Lin-Schmidt, W. Chen, T.J. Carpenter, A. Zong, W. Wang, D.L. Heald, Development of a quantitative relationship between CAR-affinity, antigen abundance, tumor cell depletion and CAR-T cell expansion using a multiscale systems PK-PD model, MAbs 12 (1) (2020) 1688616, http://dx.doi.org/10.1080/19420862.2019.1688616.

[54] S. Sabir, O. León-Triana, S. Serrano, R. Barrio, V.M. Pérez-García, Mathematical model of CAR T-cell therapy for a B-cell lymphoma lymph node, Bull. Math. Biol. 87 (3) (2025) 1–33, http://dx.doi.org/10.1007/s11538-025-01417-1.

[55] X. Zhang, L. Zhu, H. Zhang, S. Chen, Y. Xiao, CAR-T cell therapy in hematological malignancies: Current opportunities and challenges, Front. Immunol. 13 (2022) http://dx.doi.org/10.3389/fimmu.2022.927153.

[56] C.W. Freyer, D.L. Porter, Advances in CAR-T therapy for hematologic malignancies, Pharmacotherapy 40 (8) (2020) 741–755, http://dx.doi.org/10.1002/phar.2414.

[57] A.K. Valiullina, E.A. Zmievskaya, I.A. Ganeeva, M.N. Zhuravleva, E.E. Garanina, A.A. Rizvanov, A.V. Petukhov, E.R. Bulatov, Evaluation of CAR-T cells' cytotoxicity against modified solid tumor cell lines, Biomedicines 11 (2) (2023) 626, http://dx.doi.org/10.3390/biomedicines11020626.

[58] F. Marofi, R. Motavalli, V.A. Safonov, A. Jafarzadeh, M. Farhadi, M. Alijani, R. Fadaei, S. Salehi, M.H. Moghadam, M. Ebrahimi, et al., CAR-T cells in solid tumors: challenges and opportunities, Stem Cell Res. Ther. 12 (1) (2021) http://dx.doi.org/10.1186/s13287-020-02128-1.

[59] K. Newick, S. O'Brien, E. Moon, S.M. Albelda, CAR-T cell therapy for solid tumors, Annu. Rev. Med. 68 (1) (2017) 139–152, http://dx.doi.org/10.1146/annurev-med-062315-120245.

[60] D.L. Porter, B.L. Levine, M. Kalos, A. Bagg, C.H. June, Chimeric antigen receptor–modified T cells in chronic lymphoid leukemia, N. Engl. J. Med. 365 (8) (2011) 725–733, http://dx.doi.org/10.1056/NEJMoa1103849.

[61] G.L. Beatty, M. O'Hara, Chimeric antigen receptor-modified T cells for the treatment of solid tumors: Defining the challenges and next steps, Pharmacol. Ther. 166 (2016) 30–39, http://dx.doi.org/10.1016/j.pharmthera.2016.06.010.

[62] T. Qi, K. McGrath, R. Ranganathan, G. Dotti, Y. Cao, Cellular kinetics: A clinical and computational review of CAR-T cell pharmacology, Adv. Drug Deliv. Rev. 188 (2022) 114421, http://dx.doi.org/10.1016/j.addr.2022.114421.

[63] R.S. Eapen, S.G. Williams, S. Macdonald, S.P. Keam, N. Lawrentschuk, L. Au, Neoadjuvant lutetium PSMA, the TIME and immune response in high-risk localized prostate cancer, Nat. Rev. Urol. (2024) 1–11, http://dx.doi.org/10.1038/s41585-024-00913-8.

[64] F. Korell, T.R. Berger, M.V. Maus, Understanding CAR T cell-tumor interactions: Paving the way for successful clinical outcomes, Med 3 (8) (2022) 538–564, http://dx.doi.org/10.1016/j.medj.2022.05.001.

[65] M. Cazaux, C.L. Grandjean, F. Lemaître, Z. Garcia, R.J. Beck, I. Milo, J. Postat, J.B. Beltman, E.J. Cheadle, P. Bousso, Single-cell imaging of CAR T cell activity in vivo reveals extensive functional and anatomical heterogeneity, J. Exp. Med. 216 (5) (2019) 1038–1049, http://dx.doi.org/10.1084/jem.20182375.

[66] O.O. Yeku, T.J. Purdon, M. Koneru, et al., Armored CAR T cells enhance antitumor efficacy and overcome the tumor microenvironment, Sci. Rep. 7 (2017) 10541, http://dx.doi.org/10.1038/s41598-017-10940-8.

[67] E.R. Hawkins, R.R. D'Souza, A. Klampatsa, Armored CAR T-cells: The next chapter in T-cell cancer immunotherapy, Biologics: Targets Ther. (2021) 95–105, http://dx.doi.org/10.2147/BTT.S291768.

[68] L. Zhou, Y. Li, D. Zheng, Y. Zheng, Y. Cui, L. Qin, et al., Bispecific CAR-T cells targeting FAP and GPC3 have the potential to treat hepatocellular carcinoma, Mol. Ther. Oncol. 32 (2) (2024) http://dx.doi.org/10.1016/j.omton.2024.200817.